Non-parametric models in the monitoring of engine performance and condition
Part 2: non-intrusive estimation of diesel engine cylinder pressure and its use in fault detection

F Gu, P J Jacob* and **A D Ball**
School of Engineering, University of Manchester, UK

Abstract: An application of the radial basis function model, described in Part 1, is demonstrated on a four-cylinder DI diesel engine with data from a wide range of speed and load settings. The prediction capabilities of the trained model are validated against measured data and an example is given of the application of this model to the detection of a slight fault in one of the cylinders.

Keywords: angular speed, combustion diagnosis, cylinder pressure measurement, non-parametric engine model, radial basis function network

1 CYLINDER PRESSURE MEASUREMENT

The pressure waveform can be obtained either by direct measurement using a pressure transducer mounted inside a cylinder or by the use of a piezoelectric strain washer mounted beneath a cylinder head bolt. Problems are inherent with each of these techniques. Direct measurement requires a high-performance pressure transducer capable of withstanding the harsh environmental conditions that exist within the operating cylinder. Flame front transducers tend to be expensive, have relatively short lives and require considerable engine modification for their installation. Direct cylinder pressure measurement can also affect engine operation. In general, strain washers have longer lives than flame-front transducers but they too can be inconvenient to install and their output is not a direct measurement of cylinder pressure, but rather the strain in a head bolt. Age-related deterioration and adverse temperature effects can also cause problems. Both of these forms of cylinder pressure measurement require one transducer per cylinder and neither is really suited to a routine condition or performance monitoring role. Part 2 of this paper shows how the non-parametric modelling techniques derived in Part 1 may be applied to the reconstruction of cylinder pressure. Before a model may be trained to replicate an engineering system, data must be obtained that typify the behaviour of that system.

The principal concerns of Part 2 are engine testing, data acquisition and model performance assessment. In detail, Section 2 of this paper outlines the equipment used to monitor a diesel engine in a test cell and to obtain the instantaneous angular speed of the crankshaft and intrusive measurements of the cylinder pressure. In order to assess the accuracy of the model, Section 3 extracts several key engineering parameters from the pressure waveform predicted by the radial basis function network, such as the location of peak pressure and indicated mean effective pressure, and compares these parameters with values obtained from corresponding, intrusively measured waveforms.

2 ENGINE TESTS ON A DIESEL RIG

To obtain the instantaneous speed and cylinder pressure to set the parameters of the RBF network, an existing engine test facility was modified and instrumented. The specification of the test engine, a four-cylinder Ford production diesel engine, used extensively in light commercial vehicles, is given in Table 1. To allow the model to be trained and validated over a wide range of engine operation conditions, data collection was performed over a selection of speed and load settings.

The engine was loaded with a hydraulic dynamometer and was instrumented to record the operating

The MS was received on 4 August 1997 and was accepted after revision for publication on 18 May 1998.
**Corresponding author: School of Engineering, Division of Mechanical Engineering, University of Manchester, Simon Building, Oxford Road, Manchester MI3 9PL, UK.*

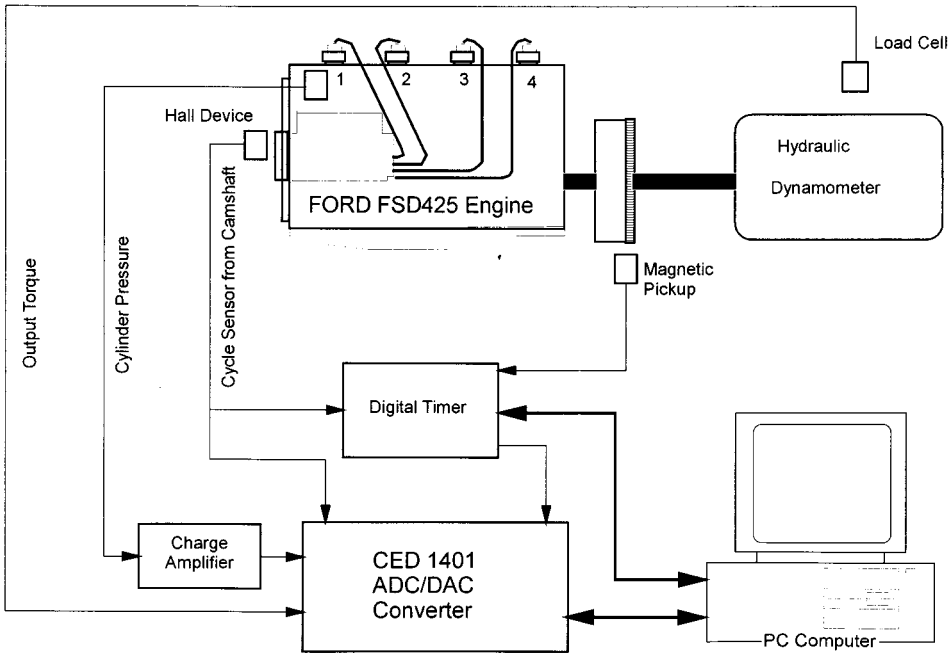

Fig. 1 Engine test instrumentation

parameters shown in Fig. 1. A flywheel mounted magnetic pickup was used to record crankshaft angular velocity, and a Hall effect device on the bottom pulley provided a timing reference point at TDC (top dead centre) of cylinder 1. The dynamometer reaction torque was measured with a load cell, and the pressure in cylinder 1 was detected by an intrusive Kistler 6125A sensor mounted in the engine, giving high sensitivity and a non-linearity in its output of less than ± 0.2 of FSO over a measuring pressure range of 0–25 MPa and a temperature range of -50 to 350 °C.

A PC system attached to an external multichannel, high-speed analogue-to-digital (A/D) converter unit was used for data collection. The CED 1401 A/D converter had a sampling rate of 125 kHz, a full scale input of 10 V and a data resolution of 12 bit, which gives a resolution of $10^4/2^{12}$ mV. By setting the sensitivity of the pressure channel at 100 mV/bar on the charge amplifier, the 12 bit accuracy of the analogue-to-digital converter unit allows a resolution of 24 mbar in the pressure signals. The 125 kHz sampling rate gave a resolution of 0.4° of crank angle at 4000 r/min when the pressure and torque signal were collected simultaneously. The CED 1401 was also used for the measurement of average engine speed, taking a timing reference from the Hall effect device on the camshaft. The timer counter has a 20 MHz clock rate and can record 2048 samples of 16 bit data. As the flywheel starter ring gear has 108 teeth, this device has the speed resolution characteristics shown in Fig. 2. The speed resolution decreases as the engine speed increases. A 1.5 r/min resolution at an engine speed of 4000 r/min is, however, considered good enough for the test, since the engine speed variation at this speed ranges from 30 to 50 r/min.

Table 1 Specifications of the test engine

Engine type	Ford FSD 425, 2.5 litre, 4-cylinder, 4-stroke, direct injection diesel
Bore × stroke	93.67 mm × 90.54 mm
Power output	50 kW at 4000 r/min (DIN)
Torque	143 N m at 2700 r/min (DIN)
Compression ratio	19:1
Compression pressure	33.8 bar (at starter motor speed)
Injection sequence	1–2–4–3 (from timing cover)
Maximum b.m.e.p.	7.35 bar

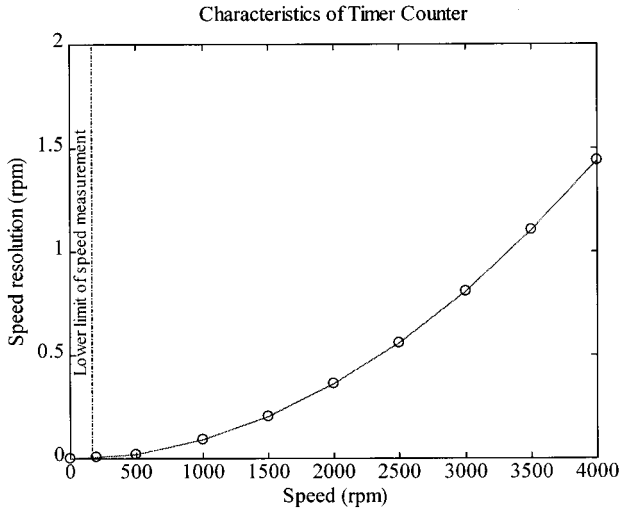

Fig. 2 Speed characteristics of timer counter

In addition to the performance, this device can also provide TTL output as it is triggered by an external pulse. This is critical to synchronize sampling of the instantaneous speed, torque and cylinder pressure.

The data collection is controlled automatically by the host computer. The average speed and torque are recorded continually throughout the test. Once the standard deviation of these two parameters is less than a predefined threshold, the computer sends a command to set the CED 1401 and the time counter so that they are awaiting a trigger signal. These two devices are then simultaneously activated by TDC index pulse.

The engine speed was controlled by adjusting the throttle position on the rack position to vary the fuel supply. The load torque could be varied by changing the braking force on the hydraulic brake. Since the model was to be validated across a wide range of speed and torque settings, data were collected with the engine running at several discrete speeds and loads. At each speed setting, torques of approximately 20, 40 and 60 N m were applied to the engine. Under each of the steady operating conditions, 10 sets of data were recorded. Each data set included the instantaneous speed trace from the crankshaft, the cylinder pressure readings and instantaneous torque. A single data set refers to the set of model inputs, i.e. the instantaneous crankshaft angular velocities measured over an entire engine cycle, and the model outputs over the same cycle.

In order that a validation of the model should be statistically valid, an independent data set, which has never at any stage been employed in conditioning the model, must be employed. To distinguish between the data set used to condition the model parameters and that used to validate the model, the conditioning data set will be labelled A, and the validatory data set B. Group A data comprised 390 engine combustion cycles and Group B data 140 combustion cycles. The pressure and speed data were measured simultaneously over a variety of engine operating settings, but with a different sampling rate for the two variables. In each pressure and speed data pair, the pressure data had 216 samples (windowed over 160° of crank angle around TDC), while the speed data had 54 samples (windowed over 180° of crank angle around TDC). Group A data were divided into two subgroups, with data taken from alternate engine cycles and each subgroup then comprising 195 cycles. One subgroup was used as the network training data to set the free model parameters. To train the network to model cylinder pressures over a wide range of load and speed settings, the 390 data items were collected at engine operating speeds between 1000 and 2600 r/min. External loads ranging from 20 to 60 N m were used. To ensure the model had sufficient interpolation accuracy between the operation settings, the speed setting was stepped in 100 r/min intervals and the load was stepped in 20 N m intervals. This led to training data with 39 cases of discrete engine operation settings.

The other subgroup of group A data was used to test the trained network. Since this test data was recorded in engine operating conditions similar to the data used to set the model parameters, this test was in fact a validation of whether the centres selected by the forward selection process had covered all of the engine operation conditions. Data group B was used only as an independent test of the network model. The 140 data sets were collected at 14 random settings over the specified speed and torque ranges. These settings often varied substantially from the training data (group A) engine settings. The data in group B had a similar structure to those in group A but were used to validate the interpolation and generalization capabilities of the network.

Several forward selection runs were performed on the data, and by making trade-offs between the reconstruction accuracy, overfitting and interpolation, the optimal model hyperparameters were identified as:

(a) radii ranging from 1000 to 10000,
(b) 100 centres, that is about 50 per cent of the training data are used as centres.

3 RBF PERFORMANCE IN CYLINDER PRESSURE PREDICTION

Figure 3 compares a selection of cylinder pressure waveforms generated from measured data and from model predictions. It can be seen that the measured and predicted pressure traces correlate well throughout the combustion process. In particular, the predicted pressure waveform reflects the early combustion phase very closely, despite the fact that this phase exhibits rapid pressure variation and is highly non-stationary. Additionally, over a range of different engine operating conditions and engine cycles, the predicted and measured waveforms remain consistent. A more detailed comparison can be made using a variety of parameters derived from the pressure waveform, of which the indicated mean effective pressure (i.m.e.p.), peak pressure and maximum rate of pressure rise are among the most frequently used in conventional engine combustion analysis.

4 COMBUSTION RELATED ENGINE PERFORMANCE INDICATORS

Conventionally the engine combustion process is characterized and its performance is assessed by the rate of heat release [**1–3**]. This can be written as

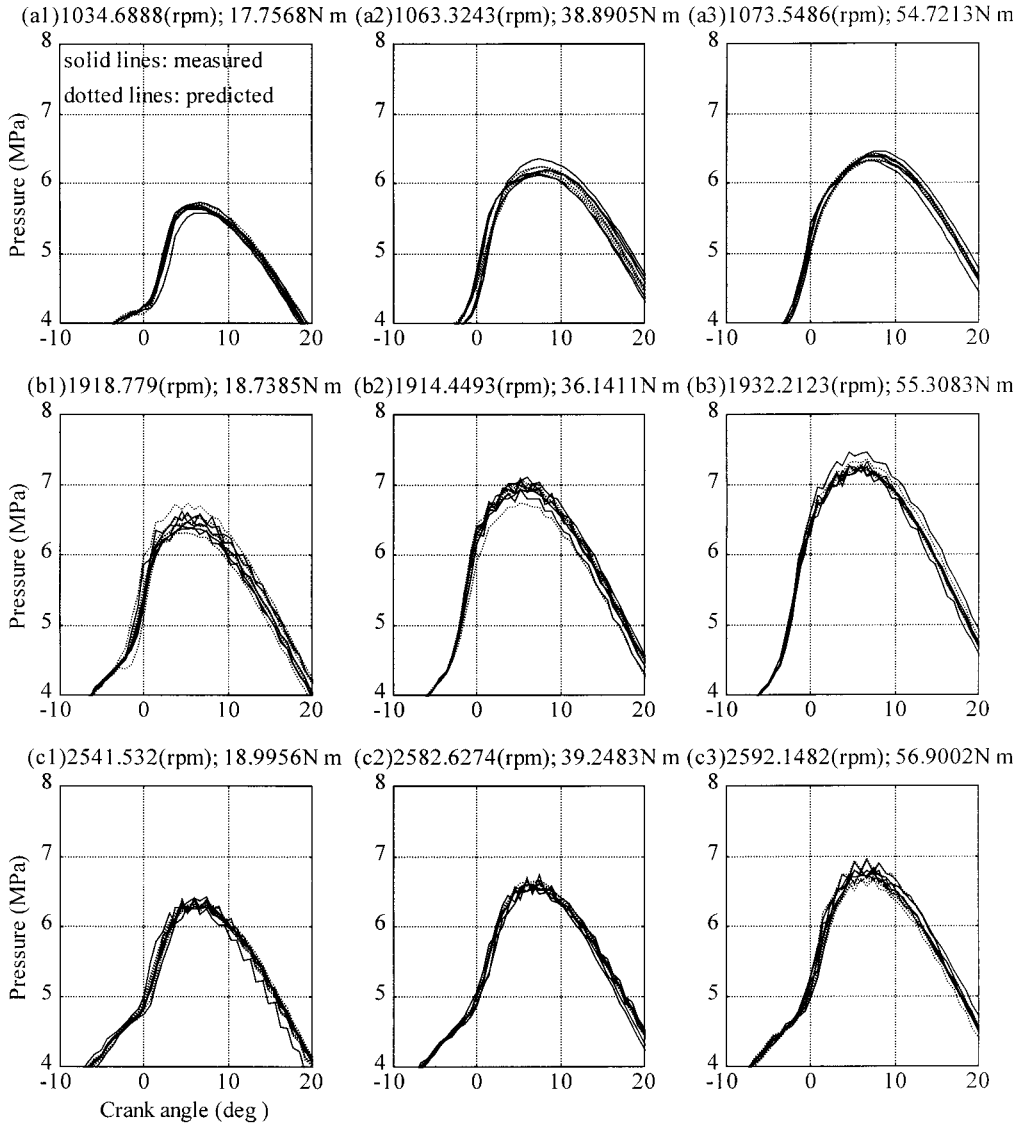

Fig. 3 Measured and predicted cylinder pressure waveforms zoomed around peak (each graph shows five directly measured pressure waveforms and five model predicted waveforms)

$$\frac{\mathrm{d}Q_n}{\mathrm{d}\theta} = \frac{\gamma}{\gamma - 1}\frac{\mathrm{d}V}{\mathrm{d}\theta}P + \frac{V}{\gamma - 1}\frac{\mathrm{d}P}{\mathrm{d}\theta} \tag{1}$$

Equation (1) explicitly shows that the rate of net heat release $\mathrm{d}Q_n/\mathrm{d}\theta$ depends upon the cylinder pressure waveform P, the rate of pressure variation with respect to the crank angle $\mathrm{d}P/\mathrm{d}\theta$, and the specific heat ratio γ, which needs to be calculated from the pressure waveform [**1**, **3**]. The close correlation between heat release and cylinder pressure makes the pressure waveform a fundamental indication in assessing combustion. Specifically, the following key assessment parameters are often extracted from cylinder pressure waveforms:

(a) peak pressure $P_{\max}$,
(b) location of peak pressure (LPP),
(c) maximum rate of pressure rise and its location,
(d) indicated mean effective pressure (i.m.e.p.).

These parameters provide a useful basis for comparison of measured and predicted cylinder pressures, particularly because they emphasize the form of the cylinder pressure waveform around the combustion region. In the following subsections, in which such comparisons are made, the stochastic nature of the combustion process is accounted for by considering cycle-to-cycle variations.

4.1 Peak pressure $P_{\max}$ and the location of peak pressure (LPP)

Figure 4 presents a comparison of peak pressures derived from measured and predicted waveforms. In the upper plot it can be seen that the predicted peak pressures correlate closely with measured values and the correlation is sufficiently accurate to allow the changes

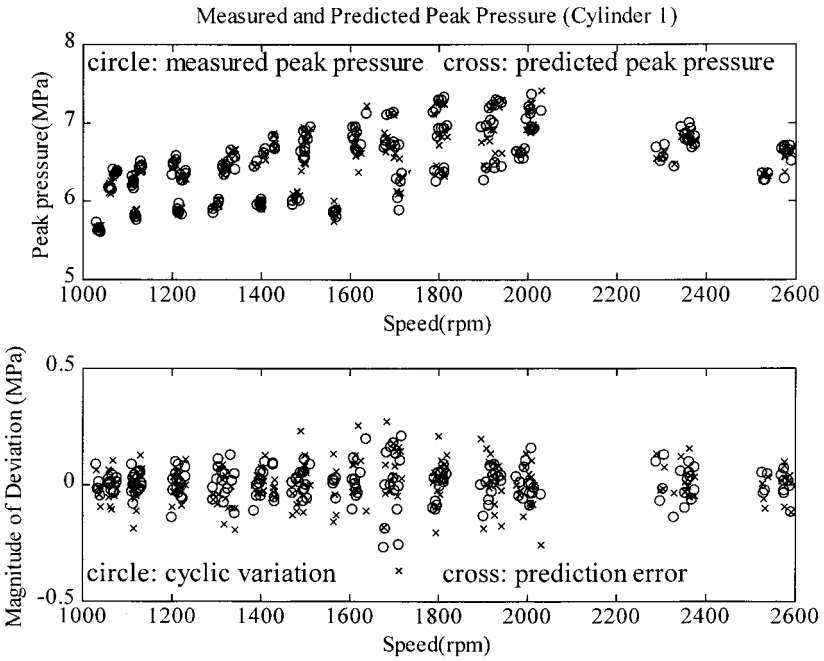

Fig. 4 Measured and predicted peak pressures

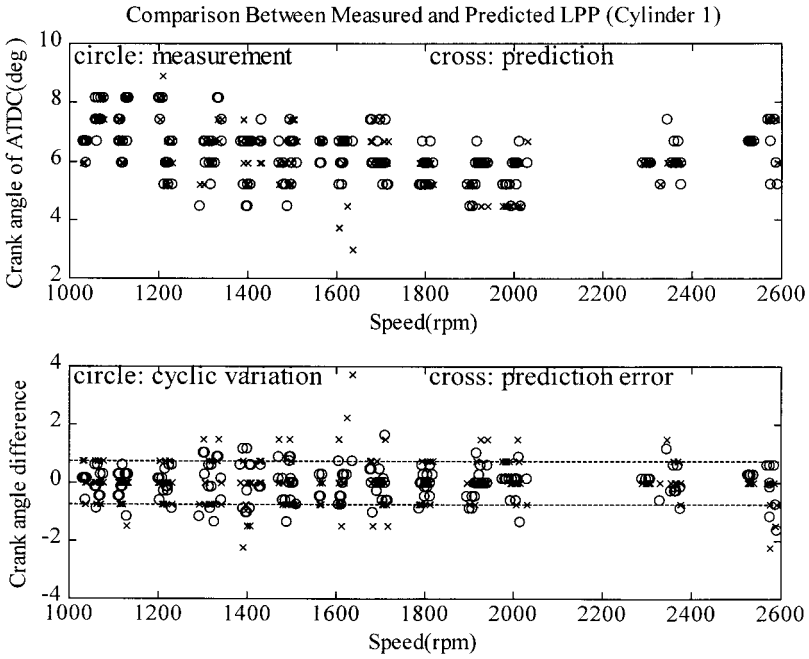

Fig. 5 Location of peak pressure (LPP)

in external load at each of the speed settings to be seen. The lower plot shows that the differences between the vast majority of measured and predicted pressure values are within ± 0.3 MPa (less than 5 per cent).

The angular location of the peak pressure (LPP) is indicative of bulk combustion phasing and it occurs slightly after the location of the maximum combustion rate, around the centre of the burn. An optimal combustion phasing generally occurs with an LPP of between 8 and 20° after the top dead centre (ATDC) [**4**]. The location of the peak cylinder pressure is often used in association with the indicated mean effective pressure (i.m.e.p.) for analysis of combustion and fuel timing characteristics.

Figure 5 compares measured and predicted LPPs and it can be seen that there exists a close similarity. The predicted LPP correlates more closely with its measured equivalent at higher engine speeds. Predicted LPP is accurate to within $\pm 0.74°$ of crank angle. Generally, LPP is optimized to vary within a 2° region of crank

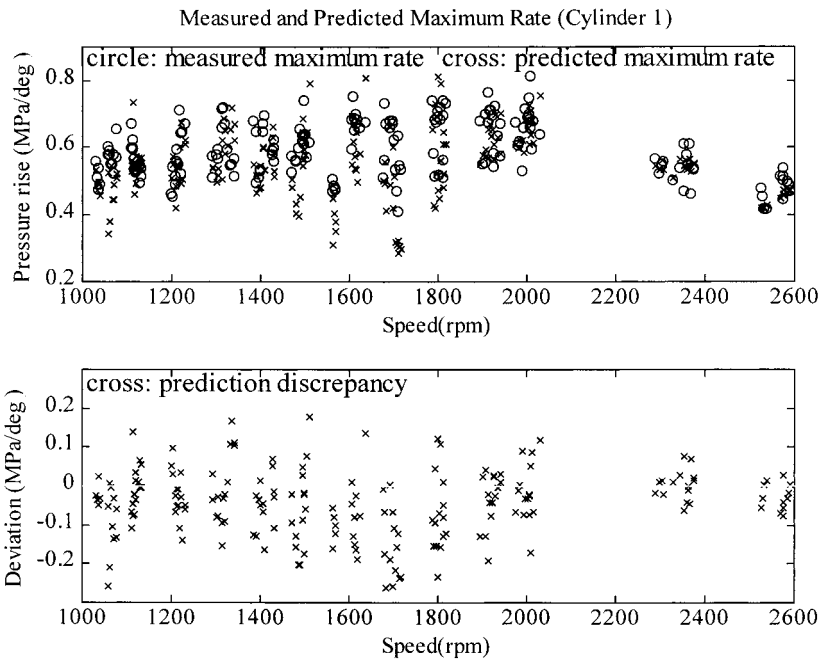

Fig. 6 Comparison of maximum rate of pressure rise

angle for this engine, and hence the predicted LPP accuracy makes it suitable for combustion phasing of the engine.

4.2 Rate of pressure rise $dP/d\theta$ and location of its maximum

The rate of pressure rise is used directly in the estimation of combustion heat release. As this is the differential of the pressure waveform, its accuracy reflects the local similarity in smoothness of the measured and predicted waveforms. Furthermore, the maximum rate of pressure rise has significant influence upon the area contained by the heat release curve and thus provides a useful basis for prediction error assessment.

Figure 6 presents a comparison between the predicted and measured maximum rates of pressure rise and their associated deviations. It can be seen that when the cyclic variation is larger, as in the speed region from 1500 to 1700 r/min, the predicted maximum rate of pressure rise is more deviant from the measured values. Discrepancies as high as 40 per cent are apparent. This does not necessarily mean that the predictions of the model are inaccurate, but rather that noise in the measured data causes a significant local roughness. Moreover, it can be seen that predictions of the maximum rate of pressure rise are in fact biased and have a tendency to exceed the values derived from measured data. It is likely that this is due to regularization of the pressure model which will tend to produce closely correlated predictions for consecutive members of a time series. Figure 7 reveals that the location of the maximum rate of pressure rise is more accurately predicted than the location of peak pressure (LPP). Almost all deviation is within $\pm 0.72°$ of crank angle (which is half the resolution of the shaft encoder).

4.3 Indicated mean effective pressure (i.m.e.p.)

Indicated mean effective pressure is the theoretical constant pressure that, if exerted during the power stroke, would produce the indicated work. On a plot of cylinder pressure against volume, i.m.e.p. is the area contained by the compression and expansion strokes divided by the displacement volume [**5**]:

$$\text{I.m.e.p.} = \frac{1}{V}\int_{\theta_1}^{\theta_2} P(\theta)\frac{\mathrm{d}V(\theta)}{\mathrm{d}\theta}\,\mathrm{d}\theta \tag{2}$$

where the range of integration is from θ_1, the onset of the compression stroke, to θ_2, the end of the power stroke.

I.m.e.p. highlights the combustion contribution to cylinder pressure and is almost linearly proportional to the brake torque. As a conventional method, it is used for quantifying combustion performance. In addition, cycle-to-cycle and cylinder-to-cylinder variation in i.m.e.p. is often used to track misfire and torque loss [**4**].

The experimental sequence referred to in Fig. 8 consists of a series of variable load, variable speed tests. Three individual loads and thirteen individual speeds, spanning the ranges identified, were used. Furthermore, six sets of cyclic data were recorded for each load–speed test to capture cycle-to-cycle variation. The upper trace in Fig. 8 should in theory appear as a series of repeated three-step 'staircases' and presents a compari-

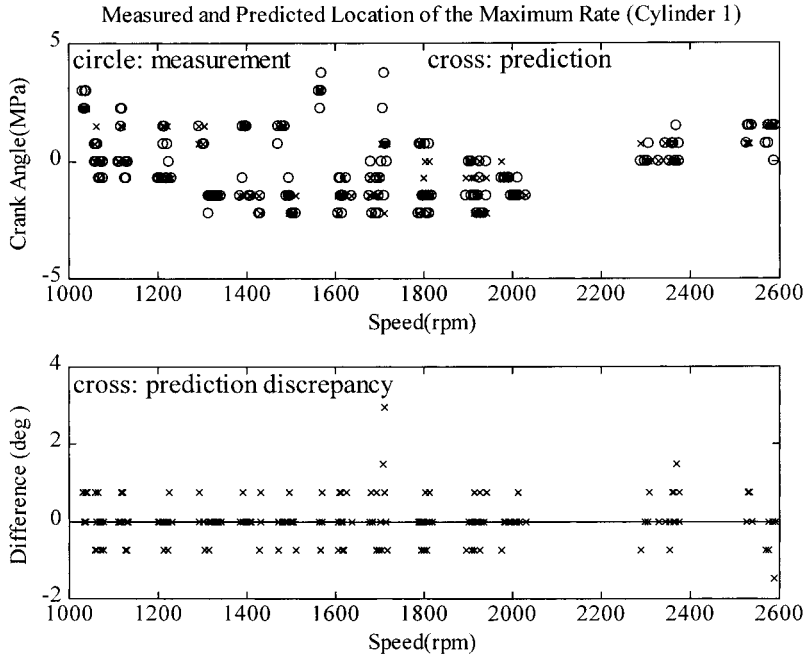

Fig. 7 Comparison of location of maximum rate of pressure rise

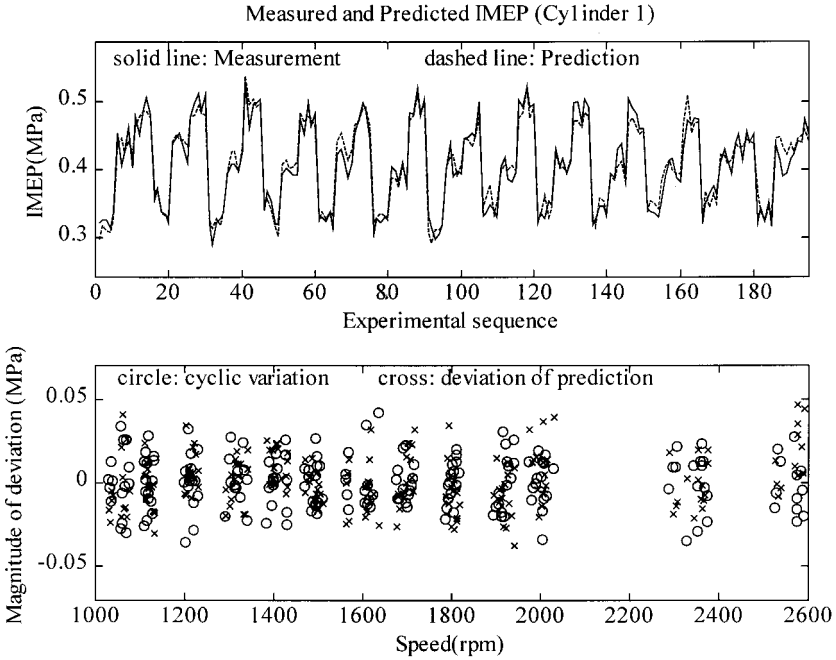

Fig. 8 Comparison of measured and predicted i.m.e.p.

son of the i.m.e.p. derived from both measurement and model prediction. It can be seen that the predicted values closely follow their measured equivalents. The step changes discriminate between the three external load settings, while the smaller changes within each step reflect the cycle-to-cycle variation at each of the engine operating conditions. The lower plot in Fig. 8 shows that the range of deviation between the predicted and measured pressures is less than ± 0.046 MPa. The variance in the model predictions can be seen to be of a similar magnitude to the variance in the data used for training.

5 FAULT DETECTION EXAMPLE

An application of waveform reconstruction was demonstrated by simulation of a minor fault in cylinder number 4. A 4 mm diameter passage was machined from the outside of the cylinder head into the combus-

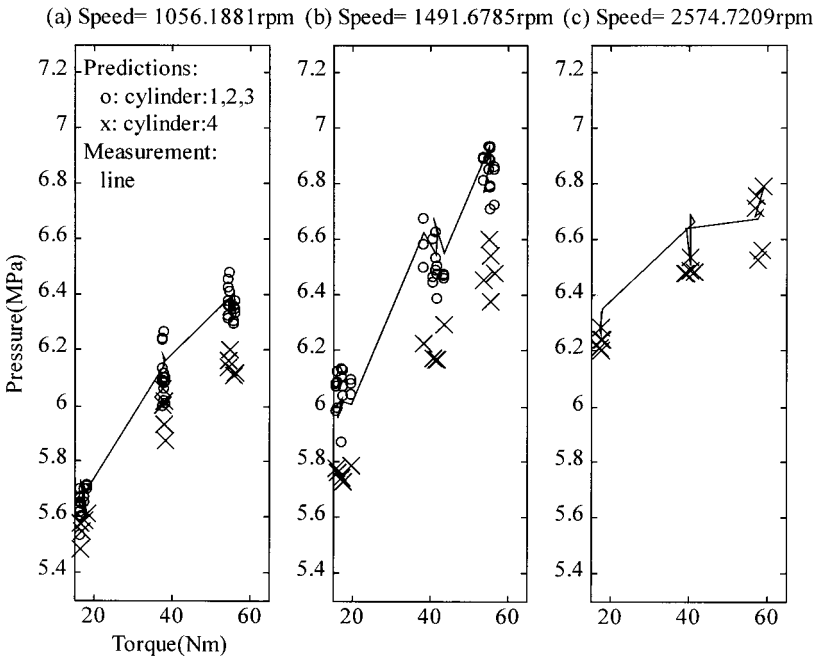

Fig. 9 Comparison of predicted and measured peak pressures for healthy and faulty cylinders

tion chamber. To the outer end of this passage was connected a short length of 4 mm bore stainless steel pipe (to permit external pressure transducers to be fitted during other types of test). The passage and extension pipe together had an approximate length of 160 mm and the end of the extension pipe was plugged to seal the combustion space. Owing to the extra volume, 2.0 cm^3, caused by the passage and pipe, the effective volume of the combustion chamber was slightly larger than normal and the compression ratio was effectively reduced from 19.0:1 to 18.0:1. Data were collected using the procedure described in Section 2. In this case, the instantaneous angular speed data were divided into four sections, each still containing 54 samples covering 180°, which were then applied separately to the RBF model to predict the pressure waveform in each of the four cylinders.

The combustion was detrimentally affected by the expansion in cylinder volume and this change in condition was reflected by the pressure waveform, which was found to deviate from the healthy cases either of the target cylinder itself or the other cylinders on the engine. As expected, the peak pressures of the waveforms from the faulty cylinder were lower than the peak pressure values from the other cylinders. Figure 9 shows the predicted peak pressures for each of the four cylinders (1, 2 and 3 healthy and 4 faulty). It also presents directly measured peak pressure in healthy cylinder number 1. There is little evident deviation and variation in the predicted peak pressure values for the three healthy cylinders. Furthermore, the predictions for one of these cylinders closely correlate with direct peak pressure measurements in that cylinder. The predicted peak pressure values for the faulty cylinder (number 4) are clearly lower than those predicted (and measured) for its healthy counterparts over corresponding speed–load settings. From the predicted peak pressure reductions of cylinder 4 it is easy to identify that this cylinder is suffering either from a slight misfire or from some other form of inefficient combustion.

6 CONCLUSIONS AND FURTHER WORK

This application of a radial basis function network to engine modelling and cylinder pressure waveform reconstruction has shown a number of promising results. Using an RBF network, the engine pressure process is described as a non-parametric model. As the information about the external load is embedded in the instantaneous speed, it can be assumed that the instantaneous speed signature is the only required input to this model. This assumption has been empirically validated by this study. To ensure accuracy in the reconstruction of the pressure waveform, it has been shown that the network should be trained with an appropriate density of training data spread over the operating speed–load plane. Intervals of 100 r/min and 20 N m gave satisfactory reconstruction accuracy for diagnostic analysis. The reconstructed waveform is consistent with intrusively measured pressures over all stages of the combustion process. In terms of engineering related combustion parameters, the accuracy obtained on a cyclic basis was as follows:

(a) deviation in peak pressure of less than ± 0.3 MPa, with a standard deviation for all samples of 9.3 per cent;
(b) deviation in i.m.e.p. of less than ± 0.046 MPa, with a standard deviation of 1.6 per cent;
(c) deviation in the maximum rate of pressure of less than ± 0.20 MPa/degree, with a standard deviation of 7.2 per cent;
(d) deviation in the location of peak pressure (LPP) of less than ± 2 crank degrees;
(e) deviation in the location of maximum pressure rise of less than ± 1 crank degree.

Further work is still to be undertaken on the core technology of the model. This should address the following issues:

1. Owing to the local applicability of the submodels contained in each RBF neuron, large networks must be used in order to obtain high accuracy in their predictions. A large network requires a correspondingly large library of training examples to ensure that free model parameters are set with statistical significance, makes heavy demands on machine resources and is slow both in recall and training. Further research should be undertaken to derive algorithms leading to more parsimonious networks with fewer free parameters.
2. Fifty-four samples of vibration data over a single engine cycle were taken as an input vector on which to condition the model predictions. However, much of the information in the space generated by these vectors is highly redundant. Research should be undertaken to identify projections on to a subspace allowing for concise representation of the information in the input domain. This would allow for smaller models with fewer inputs, requiring less training data to set free parameters. Furthermore, compact models will run faster and should be usable in real time (provided that the recall code is implemented in software to run on DSP chips).
3. Twisting of the crankshaft as the engine is placed under dynamic load conditions means that the geometry of the engine is not invariant. Such geometrical variation under acceleration and dynamic load means that the current model cannot be applied to an engine operating under such conditions. The variation in the engine geometry must be accounted for by extending the model input vectors to cover a number of engine cycles.

REFERENCES

1 **Hayves, T. K.** and **Savage, L. D.** Cylinder data acquisition and heat release analysis on a personal computer. SAE paper 860029, 1986, pp. 1–9.
2 **Rocco, V.** D.I. diesel engine in-cylinder pressure data analysis under TDC setting error. SAE paper 930595, 1993, pp. 41–49.
3 **Stone, R.** *Introduction to Internal Combustion Engines*, 2nd edition, 1995 (Society of Automotive Engineers, Warrendale, Pennsylvania).
4 **Randolph, A. L.** Cylinder pressure-based combustion analysis in race engines. SAE paper 942487, 1994.
5 **Lancaster, D. R., Krieger, R. B.** and **Lienesch, J. H.** Measurement and analysis of engine pressure data. SAE paper 750026, 1975.